Signal Fusion-Based Algorithms to Discriminate Between Radar Targets and Deception Jamming in Distributed Multiple-Radar Architectures

Shanshan Zhao, Linrang Zhang, Yu Zhou, and Nan Liu

***Abstract*— The potential abilities of distributed multiple-radar architectures in the electronic counter–countermeasure are analyzed based on the difference between target echoes and deception jamming in spatial scattering properties. The deception signals received by different receivers are fully correlated, while the correlation of target echoes varies gradually with the interval of view angles. According to this difference, the thought of signal fusion is first adopted and a corresponding algorithm is proposed to discriminate the deception jamming from radar targets in the Neyman–Pearson sense. In this algorithm, active false targets are identified by correlation tests between arbitrary two targets' complex envelopes in different receivers. To evaluate its discrimination performance, the theoretical expression for the rejection probability of false targets is derived. Simulations verify the feasibility of the new algorithm and its performance improvement over the existing data fusion-based methods. The merit of the method lies in that it can discriminate deception signals generated by arbitrary modulation and can be used in series with data fusion-based methods to improve discrimination performance further.**

***Index Terms*— Distributed multiple-radar architecture, deception electronic counter-countermeasure, signal fusion, spatial scattering property.**

I. Introduction

RADAR architectures employing multiple, widely distributed stations have been introduced recently [1]. The distributed multiple-radar architectures can exploit the spatial diversity of target scatterers supported by the system configuration. Multiple-input multiple-output (MIMO) radar systems with widely separated antennas [2]–[4] and multistatic/multisite radar systems [5] are examples of such operational architectures. These systems have been shown to offer significant advantages over monostatic radar in various aspects of radar applications, such as moving target detection [6], direction finding [7] and target localization [1], [8]. However, the practical system always suffers complicated electromagnetic environment. Different kinds of jamming may degrade the radar operation performance and even exhaust the system resources. Therefore, more attentions should be paid to their potential abilities in the electronic counter-countermeasure (ECCM), which is of vital importance to the survival and operation performance of radar systems in electronic warfare [9].

Deception electronic countermeasure (ECM), as an effective category of ECM techniques, mainly creates deceptive targets to mask useful information or saturate the target extraction and tracking algorithms [10]. With the development of digital radio frequency memory (DRFM) [11], the active false targets (FTs) retransmitted by deception jammers would be highly correlated with physical target (PT) echoes and probably overlap with the echoes in both time and frequency domain, which will significantly enhance its deception. Several ECCM strategies have been proposed to combat deception jamming. In monostatic radar, pulse diversity [12]–[14], polarization character [15], motion feature [16]–[18] and DRFM quantization error [19], [20] are used to discriminate FTs. However, the ECCM ability of monostatic radar is limited with its single view angle and deficient information obtained.

Therefore, we resort to distributed multiple-radar architectures, which have natural advantage in countering deception jamming because of its spatial diversity [21]. A jammer can hardly generate range deception signals with matched range relationship to each station opening a way to counter range deception jamming. Two identification methods of FTs, respectively in multistatic radar and netted radar, are presented based on data correlation algorithm in [22] and [23]. As regards velocity deception jamming, ECCM strategies are proposed utilizing the fact that Doppler frequencies to all stations are generally not equal for PTs, but equal for velocity deception jamming [24], [25]. However, it is worth noting that most anti-jamming methods available in distributed multiple-radar architectures are implemented by data fusion processing. Considering that lots of information (e.g., amplitude, phase of target echoes) has been indubitably discarded in the process of mensuration, the existing approaches do not fully explore the anti-jamming abilities of distributed multiple-radar architectures. It is desired to counter deception jamming by signal fusion that is defined as a direct fusion of radar echoes with less information loss compared with data levels.

The essence of ECCM techniques against deception jamming is to discriminate FTs from PTs based on their differences. Except for the range and velocity information used in the existing data fusion-based methods, spatial scattering properties can also be utilized to counter deception jamming,

Manuscript received April 3, 2015; revised May 25, 2015; accepted May 26, 2015. Date of publication June 3, 2015; date of current version September 14, 2015. This work was supported by the National Natural Science Foundation of China under Grant 61001213, Grant 61301281, and Grant 61301285. The associate editor coordinating the review of this paper and approving it for publication was Dr. Lorenzo Lo Monte.

The authors are with the National Laboratory of Radar Signal Processing, Xidian University, Xi'an 710071, China (e-mail: zhaoshanshan025@163.com; lrzhang@xidian.edu.cn; zhouyu@mail.xidian.edu.cn; liunaneoe@163.com).

Color versions of one or more of the figures in this paper are available online at http://ieeexplore.ieee.org.

Digital Object Identifier 10.1109/JSEN.2015.2440769

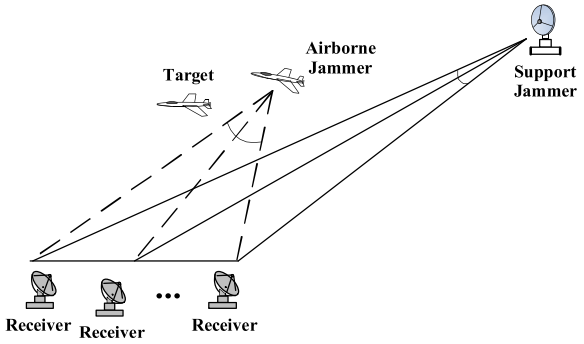

Fig. 1. Illustration of deception jamming.

which is indicated by the complex amplitude of targets and is truly a characteristic existing in signal levels. Due to spatial variations of radar cross section (RCS), the correlation of target echoes in different receivers varies gradually with the interval of view angles from complete correlation to independence [26]. On the contrary, deception signals received by different antennas are fully correlated despite the differences in signal strength caused by antenna gain and path loss effect. This difference in spatial scattering properties always exists unless the target echoes of PTs are fully correlated, which serves as the theoretical basis for our discrimination method.

The main contribution of this paper is a signal fusion-based anti-deception jamming strategy in distributed multiple-radar architectures. The strategy discriminates active false targets from physical targets based on their differences in the spatial scattering property. The discrimination method is implemented with the rejection probability of PTs being constant. Theoretical performance analysis is given, and the closed-form approximate expression for the rejection probability of FTs is derived. Specifically, the dominant merit of the approach lies in that it works for FTs generated by deception signals with arbitrary modulation, since the modulation strategies do not affect spatial scattering properties of FTs. What worth noting is that the new algorithm is performed before mensuration, and counters deception jamming by signal fusion. After being countered by our method, FTs can be identified using the existing data fusion-based approaches to raise the discrimination ratio of FTs further. The computational complexity of data fusion can be considerably reduced, owing to the fact that most FTs have been removed.

The rest of the paper is organized as follows. Section II introduces the signal model of deception jamming and PTs in distributed multiple-radar architectures. In section III, the feasibility of discriminating FTs based on the difference in the spatial scattering property is analyzed in theory. In section IV, the signal fusion-based discrimination method is proposed, and its theoretical performance analysis is given. Section V presents the simulation results for two typical scenarios. Finally, conclusions are drawn in Section VI.

II. Signal Model

As shown in Fig. 1, the deception jamming can be implemented by support jammers or airborne jammers. The support jammer has better directivity due to larger aperture, but is always far away from the radar. The airborne jammer can be nearer to the radar, but its directivity is usually poor with the limit of its aperture. Therefore, the mainlobe of the jammers will always illuminate a large area.

A radar system with one transmit and N receive radars is located in this illuminated area, forming a $1 \times N$ distributed multiple-radar architecture, all of which can receive the deception jamming. K extended physical targets (PTs) are assumed, and M active false targets (FTs) are generated by deception jammer to protect these PTs, which might be range deception, Doppler deception, angle deception, et al.

It is assumed that the synchronization of time, frequency and phase between multiple radars has been finished [27]–[29]. Let $r_n(t,q)$ be the signal received by the n-th receiver, where t is the fast-time domain and q denotes the slow-time domain. In general, the received signal $r_n(t,q)$ is the superposition of the echoes reflected by PTs $s_n(t,q)$, deception signals $j_n(t,q)$, and the internal noise $n_n(t,q)$,

$$r_n(t,q) = s_n(t,q) + j_n(t,q) + n_n(t,q), \quad n = 1,2,\ldots,N \tag{1}$$

where, $0 \le t \le T_p$, T_p is the length of a pulse repetition interval (PRI). $q = 1, 2, ..., Q$, Q is the number of the PRIs.

Denote by $R_{kn}^{(PT)}$ the range sum along the path transmitter – target k– receiver n. The ideal target echoes $s_n(t,q)$ can be simply modeled as

$$s_n(t,q) = \sum_{k=1}^{K} \alpha_{kq}^n s\left(t - R_{kn}^{(PT)} \Big/ c\right) \exp(-j2\pi R_{kn}^{(PT)} / \lambda) \tag{2}$$

where $s(t)$ is the transmitted signal, c the speed of light, λ the wavelength of the transmitted signal. α_{kq}^n is the complex amplitude of target signal which is related to the spatial scattering property. Considering a target conforms to the Swelling case II model, α_{kq}^n is modeled as a complex Gaussian distributed random variable with zero mean and variance $\sigma_{k,n}^2$, i.e., $\alpha_{kq}^n \sim \mathcal{CN}(0, \sigma_{k,n}^2)$. And the complex amplitudes in different PRIs are independent identical distributed (i.i.d.).

Assume that the carrier frequency of deception signal is the same as that of the radar transmitted signal. The deception signals $j_n(t,q)$ can be written as

$$j_n(t,q) = \sum_{m=1}^{M} \beta_{mq}^n J_m\left(t - R_n^{(J)} \Big/ c\right) \exp(-j2\pi R_n^{(J)} / \lambda) \tag{3}$$

where, β_{mq}^n is the complex amplitude of the received signal which is determined by the jamming energy and the path loss. $J_m(t)$ is the deception signal used to generate the m-th FT. $R_n^{(J)}$ is the Euclidean distance from the jammer to receiver n. As to a FT, its complex amplitude β_{mq}^n is determined by the amplitude modulation of the deception signal, which is always unknown to radars. In this paper, β_{mq}^n are modeled as random variables with unknown distributions, but are assumed i.i.d. for brevity with their average power as $\xi_{m,n}^2$, i.e., $E[(\beta_{mq}^n)^2] = \xi_{m,n}^2$.

The internal noise $n_n(t,q)$ is often assumed to be independent with other components, uncorrelated over different receivers and modeled as a complex Gaussian distributed random variable with zero mean and variance σ_n^2, i.e. $n_n(t,q) \sim \mathcal{CN}(0,\sigma_n^2)$.

In each receiver, the processing procedure is the same. The received signal is pulse compressed first. The energy of PTs will concentrate on K peaks. At the same time, M peaks would be formed by deception signal because of its match to the transmitted signal. As a result, M FTs are generated. Then, target detection is taken in order, and $K+M$ targets will be detected in each receiver, including K PTs and M FTs.

Spatial scattering properties can be reflected by mutual correlation of target echoes [26]. For every target, the slow-time complex amplitude sequence (SCAS) is introduced to describe the correlation, which is composed of the complex amplitude of the targets during several consecutive PRIs in the range cell where the target exists. The SCAS of the p-th target in receiver n can be described by

$$\boldsymbol{B}_p^n = \begin{cases} [\alpha_{p1}^n, \alpha_{p2}^n, ..., \alpha_{pq}^n, ..., \alpha_{pQ}^n]^T, & \text{if the } p\text{-th target is a PT} \\ [\beta_{p1}^n, \beta_{p2}^n, ..., \beta_{pq}^n, ..., \beta_{pQ}^n]^T, & \text{if the } p\text{-th target is a FT} \end{cases} \tag{4}$$

where $p = 1, 2, ..., K+M$, $q = 1, 2, ..., Q$, Q is the number of PRIs in a SCAS. The superscript "T" denotes the transpose operator.

Based on the definition of SCAS, for each detected target, its complex envelopes during several consecutive PRIs in its existing range cell are collected to compose a sequence. However, with the internal noise existing, the obtained sequence is the SCAS mixed with the noise sequence, defined as the slow-time complex envelope sequence (SCES). Here, it is assumed that the velocity of targets is not large enough to cause range migration, and therefore the detected targets stay in the same range cell during the PRIs used to compose SCESs. Let $\boldsymbol{A}_p^n$ be the SCES of the p-th targets in receiver n,

$$\boldsymbol{A}_p^n = \boldsymbol{B}_p^n + \boldsymbol{W}^n \tag{5}$$

where $\boldsymbol{W}^n$ is a noise sequence, with its distribution as $\boldsymbol{W}^n \sim \mathcal{CN}(0, \sigma_n^2 \mathbf{I}_{Q\times Q})$, $\mathbf{I}$ denotes the identity matrix, for $\forall n \neq n'$, $E[(\boldsymbol{W}^n)^H \boldsymbol{W}^{n'}] = 0$, the superscript "$H$" denotes the Hermitian operator.

Finally, the SCES $\boldsymbol{A}_p^n$ of every target in N receivers are delivered to the fusion center where the information are fused and jointly processed to discriminate FTs.

III. Feasibility Analysis

In order to verify the feasibility of discriminating FTs from PTs based on their difference in spatial scattering properties, the mutual correlation of SCESs $\boldsymbol{A}_p^n$ in different receivers is analyzed in theory. Take the n-th and the n'-th receiver for an example. With the corresponding relations among the detected targets in each receiver uncertain, a traverse for all possible combinations $\{\boldsymbol{A}_p^n, \boldsymbol{A}_{p'}^{n'} | \forall p, \forall p' = 1, 2, ..., K+M\}$ is inevitable. Therefore, the problem is formulated here as a multiple hypothesis testing (MHT) problem with five hypotheses.

- Under the null hypothesis (H_0), it is assumed that the combination consists of two SCESs originating from the same PT.
- Under the first hypothesis (H_1), it is assumed that the combination consists of two SCESs originating from two different PTs.
- Under the second hypothesis (H_2), it is assumed that the combination consists of two SCESs originating from a PT and a FT.
- Under the third hypothesis (H_3), it is assumed that the combination consists of two SCESs generated by different deception signals.
- Under the fourth hypothesis (H_4), it is assumed that the combination consists of two SCESs generated by the same deception signal.

Under H_0, $\boldsymbol{A}_p^n$ and $\mathbf{A}_{p'}^{n'}$ correspond to one PT. Due to the independence of the noise, their mutual correlation of SCESs can be written as

$$E\left[(\boldsymbol{A}_p^n)^H \boldsymbol{A}_{p'}^{n'}\right] = E\left[(\boldsymbol{B}_p^n)^H \boldsymbol{B}_{p'}^{n'}\right] \tag{6}$$

As referred in [26], a uniform formula has been derived to estimate the correlation coefficient $\rho_{nn'}$ of $\{\alpha_{pq}^n\}_{q=1}^Q$ for one PT in receiver n and n', which depends on carrier frequency f_m, target size D and view angle interval of these two receivers $\Delta\beta_{nn'}$:

$$\rho_{nn'} = \frac{E[(\boldsymbol{B}_p^n)^H \boldsymbol{B}_{p'}^{n'}]}{Q \cdot \sqrt{\sigma_{p,n}^2 \sigma_{p',n'}^2}} = J_0(2\pi D f_m \sin(\Delta\beta_{nn'}/2)/c) + J_2(2\pi D f_m \sin(\Delta\beta_{nn'}/2)/c), \quad \forall n \neq n' \tag{7}$$

where $J_0(\cdot)$ and $J_2(\cdot)$ are the first kind Bessel functions of the zero- and the second-order, respectively.

Fig. 2 shows the spatial distribution of the correlation coefficient for a fixed 1×2 distributed multiple-radar system with transmitter located at the origin, where $f_m = 3$GHz, $D = 15$m. Two receivers are located at coordinates $(\pm 300, 0)$m, and both can receive the jamming signals. It is obvious that the target in most parts has been decorrelated, and the correlation coefficient is less than one. The existing difference between targets and deception signals in spatial

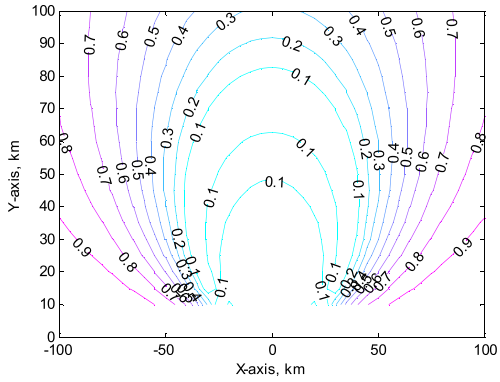

Fig. 2. Correlation coefficient of target echoes.

scattering properties can be utilized to discriminate deception jamming.

According to (7), the mutual correlation of SCESs under H_0 can be given by

$$E\left[(\boldsymbol{A}_p^n)^H \boldsymbol{A}_{p'}^{n'}\right] = \rho_{nn'} \cdot Q\sqrt{\sigma_{p,n}^2 \sigma_{p',n'}^2}, \quad n \neq n' \tag{8}$$

Under H_1, $\boldsymbol{A}_p^n$ and $\boldsymbol{A}_{p'}^{n'}$ correspond to two different PTs. Different targets generally have independent spatial fluctuations, the mutual correlation of SCESs under H_1 is

$$E\left[(\boldsymbol{A}_{p|\mathrm{PT}}^n)^H \boldsymbol{A}_{p|\mathrm{PT}}^{n'}\right] = E\left[(\boldsymbol{B}_{p|\mathrm{PT}}^n)^H \boldsymbol{B}_{p|\mathrm{PT}}^{n'}\right] = 0, \quad n \neq n' \tag{9}$$

Under H_2, $\boldsymbol{A}_p^n$ and $\boldsymbol{A}_{p'}^{n'}$ correspond to a PT and a FT. Similarly to H_1, the mutual correlation under H_2 is

$$E\left[(\boldsymbol{A}_{p|\mathrm{PT}}^n)^H \boldsymbol{A}_{p|\mathrm{FT}}^{n'}\right] = E\left[(\boldsymbol{B}_{p|\mathrm{PT}}^n)^H \boldsymbol{B}_{p|\mathrm{FT}}^{n'}\right] = 0, \quad n \neq n' \tag{10}$$

Under H_3, $\boldsymbol{A}_p^n$ and $\boldsymbol{A}_{p'}^{n'}$ correspond to two FTs generated by different deception signals. Their mutual correlation is generally unknown based on the established model. If the complex amplitudes of FTs have independent fluctuations, $E\left[(\boldsymbol{A}_p^n)^H \boldsymbol{A}_{p'}^{n'}\right] = 0, n \neq n'$. If not, $E\left[(\boldsymbol{A}_p^n)^H \boldsymbol{A}_{p'}^{n'}\right] \neq 0$, $n \neq n'$.

Under H_4, $\boldsymbol{A}_p^n$ and $\boldsymbol{A}_{p'}^{n'}$ correspond to one FT generated by the same deception signal. The complex amplitudes $\{\beta_{pq}^n\}_{q=1}^Q$ of one FT are completely correlated. Hence, the SCASs in different receivers for FTs are linear related,

$$\boldsymbol{B}_p^n = k \cdot \boldsymbol{B}_{p'}^{n'}, \quad n \neq n' \tag{11}$$

where $|k| = \sqrt{\xi_{p',n'}^2 / \xi_{p,n}^2}$. Note that varying Doppler modulation across slow-time will influence the correlation, but is not considered here, since the modulated Doppler frequency usually remains unchanged or varies slightly and the slight Doppler variation has little effects on the correlation.

The mutual correlation of SCESs under H_4 can be given by

$$E\left[(\boldsymbol{A}_p^n)^H \boldsymbol{A}_{p'}^{n'}\right] = E\left[(\boldsymbol{B}_p^n)^H \boldsymbol{B}_{p'}^{n'}\right] = Q\sqrt{\xi_{p,n}^2 \xi_{p',n'}^2}, \quad n \neq n' \tag{12}$$

Combining the obtained results, the mutual correlation of $\mathbf{A}_p^n$ and $\boldsymbol{A}_{p'}^{n'}$ can be unified as

$$E\left[(\boldsymbol{A}_p^n)^H \boldsymbol{A}_p^{n'}\right] = \kappa \cdot Q\sqrt{\varsigma_{p,n}^2 \varsigma_{p',n'}^2}, \quad n \neq n' \tag{13}$$

where $\varsigma_{p,n}^2$ are the average power of the complex amplitude of targets. For a PT, $\varsigma_{p,n}^2 = \sigma_{p,n}^2$, and for a FT, $\varsigma_{p,n}^2 = \xi_{p,n}^2$. κ is the correlation coefficient between corresponding SCASs,

$$\kappa = \begin{cases} \rho_{nn'}, & \text{under } H_0 \\ 0, & \text{under } H_1, H_2 \\ \text{unknown}, & \text{under } H_3 \\ 1, & \text{under } H_4 \end{cases} \tag{14}$$

It is obvious that the difference in the mutual correlation is caused by κ. In distributed multiple-radar architectures, the correlation coefficients generally satisfy $\rho_{nn'} < 1$ as shown in Fig. 2. That is to say, for a PT, its mutual correlation with arbitrary target in the other receivers is small. However, for a FT, there is always one target that is fully correlated with the FT under H_4. In conclusion, it is feasible to identify FTs by using correlation test based on the mutual correlation, and if a combination is tested to be H_4, it can be judged that two targets included both correspond to FTs.

IV. Discrimination Method

Mutual correlation is a statistic, and therefore its unbiased estimation is utilized to discriminate FTs in practice. Due to the limitation of the number of available samples, the estimation is a random variable with its mean as (13). According to (13), the imaginary part of the estimation tends to be zero under arbitrary hypotheses, which is useless for the discrimination. Therefore, we introduce a new measure, named correlation metric, which is defined as the real component of the estimation of mutual correlation,

$$\Omega_{pp'} = \mathrm{Re}\left((\boldsymbol{A}_p^n)^H \boldsymbol{A}_{p'}^{n'}\right), \quad \forall n \neq n' \tag{15}$$

By decomposing complex vectors into the real and image parts, the correlation metric in (15) changes to,

$$\Omega_{pp'} = (\boldsymbol{G}_p^n)^{\mathrm{T}} \boldsymbol{G}_{p'}^{n'} \tag{16}$$

with $\boldsymbol{G}_p^n = [\mathrm{Re}(\boldsymbol{A}_p^n)^T, \mathrm{Im}(\boldsymbol{A}_p^n)^T]^T$, $\boldsymbol{G}_{p'}^{n'} = [\mathrm{Re}(\boldsymbol{A}_{p'}^{n'})^T, \mathrm{Im}(\boldsymbol{A}_{p'}^{n'})^T]^T$. Note that $\Omega_{pp'}$ can be regarded as the inner product of two real-valued independent stochastic vectors. Consequently, $\Omega_{pp'}$ is a sum of $2Q$ random variables,

$$\Omega_{pp'} = \sum_{i=1}^{2Q} (g_p^n)_i (g_{p'}^{n'})_i \tag{17}$$

where $(g_p^n)_i$ and $(g_{p'}^{n'})_i$ represents the i-th component of $\boldsymbol{G}_p^n$ and $\boldsymbol{G}_{p'}^{n'}$, respectively. Assume that the energy of the real and image parts are the same and that the components of stochastic vectors $\boldsymbol{G}_p^n$ or $\boldsymbol{G}_{p'}^{n'}$ are i.i.d.. Then the added random variables $(g_p^n)_i (g_{p'}^{n'})_i$ are also independent identical distributed.

Invoking the central limit theorem, the distribution of $\Omega_{pp'}$ can be approximately normal whose mean and variance are determined by that of the added random variables. As to the approximation error, the Berry-Esseen theorem gives a bound on the maximal error [30]. The quantitative analysis of the approximation error is not given. And in the simulation, we have shown that the approximation error has little effects on the results.

The discrimination approach is firstly given in the case of two receivers $N = 2$, and the generalization to $N > 2$ is followed.

A. Correlation Test

Based on correlation metrics, correlation tests are implemented to identify FTs, which are formulated as a MHT problem. Since the distributions of correlation metrics under H_2, H_3 and H_4 are not known with the distributions of the complex amplitudes of FTs unknown, the optimal detector, likelihood ratio test, is not practical in our MHT problem.

TABLE I
MEAN AND VARIANCE OF $\Omega_{pp'}$ UNDER H_0, H_1 AND H_2

	Mean $\mu_{pp'}$	Variance $\sigma^2_{pp'}$
Under H_0	$\rho_{12}\cdot Q\sqrt{\sigma^2_{p,1}\sigma^2_{p',2}}$	$\frac{Q}{2}\left(\zeta^2_{p,1}\zeta^2_{p',2}+\rho_{12}\sigma^2_{p,1}\sigma^2_{p',2}\right)$
Under H_1	0	$\frac{Q}{2}\zeta^2_{p,1}\zeta^2_{p',2}$
Under H_2	0	$\frac{Q}{2}\zeta^2_{p,1}\zeta^2_{p',2}$

We resort to the Neyman-Pearson lemma to design the discrimination algorithm. The cost of the rejection of PTs is usually much higher than that of the acceptance of FTs. A reasonable discrimination procedure is to differentiate FTs subject to an acceptable rejection probability of PTs, named constant PTs rejection ratio.

For the MHT, PTs are included in H_0, H_1 and H_2. We combine these three hypotheses as $H = H_0\,|H_1\,|H_2$, and its opposite hypothesis $H' = H_3\,|H_4$. Then, the correlation test can be simply designed as

$$\begin{cases} H: & \Omega_{pp'} \le \eta \\ H': & \Omega_{pp'} > \eta \end{cases} \tag{18}$$

where η is the adaptive threshold to satisfy constant PTs rejection ratio, which depends on the probability density function (PDF) of correlation metrics $\Omega_{pp'}$ under H. If the correlation metric of one combination is larger than the threshold, H' holds, which means that the targets included in the combination would be all FTs. On the contrary, the targets included in the combination are judged temporarily to be PTs.

As mentioned above, the distribution of correlation metrics is approximately normal, described by $\Omega_{pp'} \sim \mathcal{N}(\mu_{pp'}, \sigma^2_{pp'})$. In order to design the adaptive threshold η, the means and variances of $\Omega_{pp'}$ under H_0, H_1 and H_2 are given in Table I, where $\zeta^2_{p,n}$ represents the average power of the components of the p-th SCES in receiver n, $n = 1, 2$.

$$\zeta^2_{p,n} = \begin{cases} \sigma^2_{p,n} + \sigma^2_n, & \text{if the } p\text{-th SCES corresponds to a PT} \\ \xi^2_{p,n} + \sigma^2_n, & \text{if the } p\text{-th SCES corresponds to a FT} \end{cases} \tag{19}$$

For a PT, it is tested in the number of $(K+M)$ correlation tests. If one of the correlation tests is judged as H', the PT will be judged as FTs. The rejection probability of PTs, denoted by P_l, should be calculated as

$$\begin{aligned} P_l &\triangleq P\{\text{rejected as FTs}\,|\text{a PT}\} \\ &= P\{\text{at least one of } (K+M) \text{ correlation tests is} \\ &\qquad \text{judged as } H'\} \\ &= 1 - P\{\Omega_{pp'} \le \eta, \forall p' = 1, 2, ..., K+M\} \\ &= 1 - P\{\Omega_{pp'} \le \eta\,|H_0\}P\{\Omega_{pp'} \le \eta\,|H_1\}^{K-1} \\ &\quad \times P\{\Omega_{pp'} \le \eta\,|H_2\}^{M} \end{aligned} \tag{20}$$

According to Table I, an equality for the threshold η can be obtained as

$$\begin{aligned} P_l &= F(\eta) \\ &\triangleq 1 - \Phi\left(\frac{\eta - \rho_{12}\cdot Q\sqrt{\sigma^2_{p,1}\sigma^2_{p',2}}}{\sqrt{Q(\zeta^2_{p,1}\zeta^2_{p',2} + \rho_{12}\sigma^2_{p,1}\sigma^2_{p',2})/2}}\right) \\ &\quad \times \Phi\left(\frac{\eta}{\sqrt{Q\zeta^2_{p,1}\zeta^2_{p',2}/2}}\right)^{K+M-1} \end{aligned} \tag{21}$$

where $\Phi(\cdot)$ stands for the cumulative distribution function of the standard normal distribution and $\Phi^{-1}(\cdot)$ is its inverse function. For a pre-set P_l, the threshold η is determined by the equality (21), but cannot be obtained directly due to the complexity. However, $F(\eta)$ is a monotonic increasing function with η, we can obtained a possible range, described by $[\eta_{\min}, \eta_{\max}]$ with

$$\eta_{\min} = \sqrt{Q\zeta^2_{p,1}\zeta^2_{p',2}/2}\cdot\Phi^{-1}\left((1-P_l)^{1/K+M}\right) \tag{22}$$

$$\begin{aligned} \eta_{\max} &= \sqrt{Q(\zeta^2_{p,1}\zeta^2_{p',2} + \rho_{12}\sigma^2_{p,1}\sigma^2_{p',2})/2} \\ &\quad \cdot\Phi^{-1}\left((1-P_l)^{1/K+M}\right) \\ &\quad + \rho_{12}\cdot Q\sqrt{\sigma^2_{p,1}\sigma^2_{p',2}} \end{aligned} \tag{23}$$

Then, binary search algorithm can be used here to obtained the value of η efficiently. The terminate condition is chosen to ensure the relative error less than a pre-set threshold, i.e., $\left|F(\hat{\eta}) - P_l\right| / P_l \le \varepsilon$.

B. Proposed Discrimination Method

According to the aforementioned correlation tests, the proposed discrimination method can be derived as the following steps.

Step 1 (Pre-processing): For a desired target size D, the correlation coefficient ρ_{12} is estimated by (7); Echoes energy and noise energy in every receivers are also estimated.

Step 2 (Correlation test): For every possible combination consisting of two SCESs in receivers 1 and 2, correlation tests are implemented using (18).

Step 3 (FTs discrimination): Once a combination is tested to be H_3 or H_4, two targets included are rejected as FTs. After all combinations have been processed, the targets left are accepted as PTs.

The complete signal processing procedure is provided in Fig. 3, including the respective processing in each receiver and the joint processing in the fusion central.

Obviously, most fusion computational costs exist in step 2, i.e. the correlation test. The calculation of the correlation metric can be simply realized by vector inner product. The computational cost of correlation test mainly depends on the calculation of the adaptive threshold, which is determined by (21) and realized by binary search algorithm. Through the simulation, we find that the search algorithm always converges within ten iterations and is computationally efficient. Besides, with adequate storage capacity, the threshold for every possible parameter can be calculated off-line and used to establish a

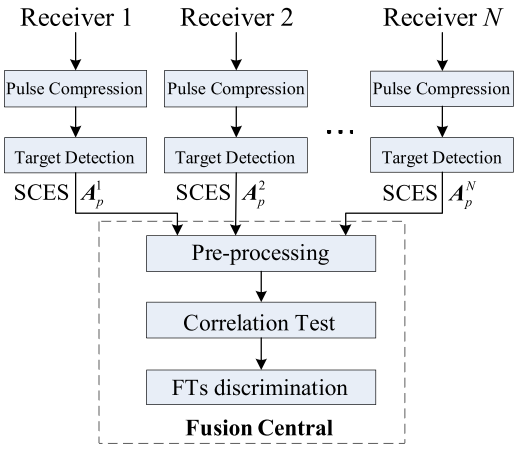

Fig. 3. The complete signal processing procedure.

threshold table. Then the determination of threshold can be simply realized by seeking the threshold table, which will largely reduce the complexity of the proposed method.

If there are more than two receivers in the distributed multiple-radar architecture, the method can be generalized. Firstly, two receivers with the longest baseline are used to identify FTs, since their discrimination performance is the best compared with the other pairs of receivers. On one hand, for all the combinations judged as FTs, coherent integration is used to obtain reference SCESs to raise the average power. These reference SCESs are used to discriminate FTs in the third receiver. On the other hand, for all the SCESs judged as PTs, the left SCESs in the third receiver are used to discriminate FTs from them using the correlation test. Finally, the combinations judged as FTs are integrated again. By analogy, the discrimination procedure for the entire distributed multiple-radar system can be accomplished.

In addition, although the proposed method is given in the case of $1 \times N$ architecture, it can be used for a distributed multiple-radar system with multiple transmit radars due to the fact that it can be regarded as a combination of multiple independent $1 \times N$ architectures.

C. Performance Analysis

To evaluate the performance of the proposed discrimination scheme, the acceptance probability of PTs (P_{PT}) and the rejection probability of FTs (P_{FT}) are introduced.

The **acceptance probability of PTs** is defined as

$$\begin{aligned} P_{PT} &\triangleq P\{\text{accepted as PTs}|\text{a PT}\} \\ &= 1 - P_l \end{aligned} \tag{24}$$

which is a constant for a previously given P_l.

The **rejection probability of FTs** is similarly defined as

$$\begin{aligned} P_{FT} &\triangleq P\{\text{rejected as FTs}|\text{a FT}\} \\ &= P\{\text{at least one of } (K+M) \text{ correlation} \\ &\qquad \text{tests is judged as } H'\} \\ &= 1 - P\{\Omega_{pp'} \le \eta, \forall p' = 1, 2, ..., K+M\} \\ &= 1 - P\{H\,|H_2\}^K P\{H\,|H_3\}^{M-1} P\{H\,|H_4\} \end{aligned} \tag{25}$$

TABLE II
MEAN AND VARIANCE OF $\Omega_{pp'}$ UNDER H_3 AND H_4

		Mean $\mu_{pp'}$	Variance $\sigma^2_{pp'}$
Under H_3	Case 1[a]	$Q\sqrt{\xi^2_{p,1}\xi^2_{p',2}}$	$\frac{Q}{2}\left(\xi^2_{p,1}\sigma_2^2 + \xi^2_{p',2}\sigma_1^2 + \sigma_1^2\sigma_2^2\right)$
	Case 2[b]	0	$\frac{Q}{2}\zeta^2_{p,1}\zeta^2_{p',2}$
Under H_4	Case 1	$Q\sqrt{\xi^2_{p,1}\xi^2_{p',2}}$	$\frac{Q}{2}\left(\xi^2_{p,1}\sigma_2^2 + \xi^2_{p',2}\sigma_1^2 + \sigma_1^2\sigma_2^2\right)$
	Case 2	$Q\sqrt{\xi^2_{p,1}\xi^2_{p',2}}$	$\frac{Q}{2}\left(\zeta^2_{p,1}\zeta^2_{p',2} + \xi^2_{p,1}\xi^2_{p',2}\right)$

[a] In case 1, the complex amplitudes of FTs have no fluctuation.
[b] In case 2, the complex amplitudes of FTs possess a normal distribution.

where, $P\{H\,|H_2\} = \Phi(\eta/\sqrt{Q\zeta^2_{p,1}\zeta^2_{p',2}/2})$, $P\{H\,|H_3\}$ and $P\{H\,|H_4\}$ are determined by the distributions of $\Omega_{pp'}$ under H_3 and H_4, respectively.

Since the distribution of the complex amplitude of FTs β^n_{pq} is unknown, it is impossible to get a general PDF of $\Omega_{pp'}$ under H_3 and H_4 for all possible distributions. If β^n_{pq} have no fluctuation, its distribution can be regarded as a one point distribution. On the other hand, β^n_{pq} might have a random fluctuation to obtain a better deception performance. Under this circumstance, the normal distribution is always a preferable choice to imitate the fluctuation of PTs.

As a result, we now try to give the theoretical expression for P_{FT} in these two cases. It has been derived that the distribution of $\Omega_{pp'}$ is approximately normal. The means and variances of $\Omega_{pp'}$ in both cases under H_3 and H_4 are given in Table II.

In case 1, the complex amplitudes of FTs have no fluctuation. The means and variances of $\Omega_{pp'}$ under H_3 and H_4 are the same. $P\{H\,|H_3\}$ and $P\{H\,|H_4\}$ can be given by

$$\begin{aligned} P\{H\,|H_3\} &= P\{H\,|H_4\} \\ &= \Phi\left(\frac{\eta - Q\sqrt{\xi^2_{p,1}\xi^2_{p',2}}}{\sqrt{Q(\xi^2_{p,1}\sigma_2^2 + \xi^2_{p',2}\sigma_1^2 + \sigma_1^2\sigma_2^2)/2}}\right) \end{aligned} \tag{26}$$

The theoretical expression for P_{FT} in case 1 can be obtained by substituting (26) into (25).

In case 2, the complex amplitudes of FTs possess a normal distribution. With the results in Table II, $P\{H\,|H_3\}$ and $P\{H\,|H_4\}$ can be obtained as

$$P\{H\,|H_3\} = \Phi\left(\eta \Big/ \sqrt{Q\zeta^2_{p,1}\zeta^2_{p',2}\Big/2}\right) \tag{27}$$

$$P\{H\,|H_4\} = \Phi\left(\frac{\eta - Q\sqrt{\xi^2_{p,1}\xi^2_{p',2}}}{\sqrt{Q\left[\zeta^2_{p,1}\zeta^2_{p',2} + \xi^2_{p,1}\xi^2_{p',2}\right]/2}}\right) \tag{28}$$

Similarly, theoretical P_{FT} in case 2 can be obtained by substituting (27) and (28) into (25).

Note that the closed-form expressions for P_{PT} and P_{FT} are obtained on the premise of *a priori* knowledge, such as the correlation coefficient of PTs, the echoes and noise

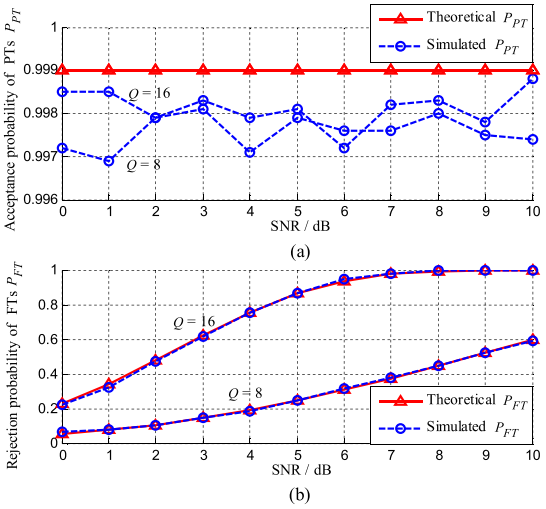

Fig. 4. (a) P_{PT} and (b) P_{FT} against SNR in case 1.

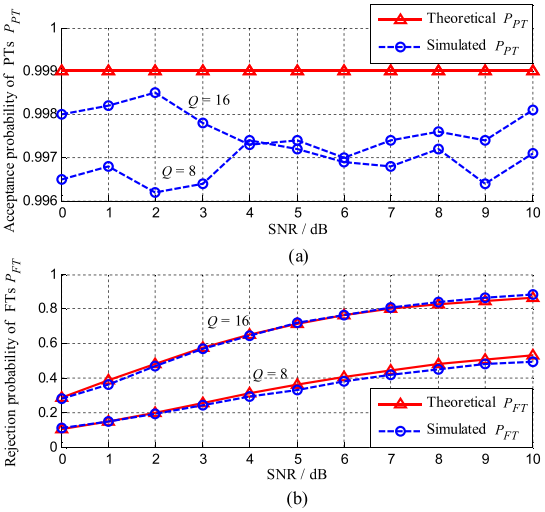

Fig. 5. (a) P_{PT} and (b) P_{FT} against SNR in case 2.

energy in every receivers, which represent a benchmark to the performance of our discrimination method. The estimation error of these parameters may inevitably lead to a deviation. Furthermore, the normal approximation for the distribution of $\mathbf{\Omega}_{pp'}$ might also draw some deviations.

V. Simulation Results

In this section, we begin with a description of the simulated scenario. We simulated a distributed multiple-radar architecture consisting of a transmitter and two separated receivers. It is assumed that only one PT is present in the joint detected area, since it does not influence the conclusion. A self-screening repeater jammer is carried, and M FTs are generated. We define signal-to-noise ratio as SNR $= \sigma_{p,n}^2/\sigma_n^2$ for the PT and jamming-to-noise ratios as JNR $= \xi_{p,n}^2/\sigma_n^2$ for FTs. Since deception jammers are not performed to jam the radar depending on the power, SNR and JNR are assumed the same in both receivers. In practice, JNR is usually larger than SNR, in which cases the discrimination performance would be better than our simulated results. Without confusion, SNR is used to represent both SNR and JNR in the simulation, unless special illustration is given. According to the fluctuation of FTs, two simulation scenarios are considered.

Case 1: The complex amplitudes of FTs have no fluctuation.

Case 2: The complex amplitudes of FTs have a fluctuation with normal distribution.

A. Monte Carlo Simulations

Monte Carlo simulations are given first to verify the feasibility of the proposed approach. We consider the presence of one FT, i.e., $M = 1$. The correlation coefficient of the PT is assumed to be 0.1, and its estimate error possesses a Gaussian distribution with zero mean and variance 0.01. The expected rejection probability of PTs is set to be 10^{-3}, i.e., $P_l = 10^{-3}$.

In Fig. 4, the acceptance probability of PTs P_{PT} and the rejection probability of FTs P_{FT} are given as a function of SNR in case 1. P_{PT} and P_{FT} are obtained by both the obtained theoretical expression and Monte Carlo simulations with 10^4 trials. The curves correspond to different values of the number of PRIs Q, where $Q = 8$ and 16. Fig. 5 reports the results in case 2 with the same parameters.

It is apparent that the simulated results of P_{PT} are close to its theoretical value in both cases, $P_{PT} = 1 - P_l = 0.999$, with a deviation less than 0.003 meaning that the proposed method can achieve a pre-set rejection probability of PTs in spite of the use of the normal approximation. Moreover, the simulated results of P_{FT} correspond to the theoretical results with little deviations caused by the estimate errors and normal approximation in both cases. All these deviations decrease with increasing value of Q, since the approximation error become smaller with more number of PRIs.

Besides, we can also see from Figs. 4 and 5 that the discrimination ratio of FTs becomes better with higher SNR and more number of PRIs due to the fact that the difference in mutual correlations under difference hypotheses is in proportion to these two parameters presented in (13).

B. Discrimination Operating Characteristic (DOC)

Except for the above two parameters, the performance also depends on the correlation coefficient of the PT and the number of FTs. In order to analyze their effects, discrimination operating characteristic (DOC) is introduced to evaluate the performance using the theoretical expression (25), which is defined as the curve of P_{FT} as a function of P_l, similar to the well-known receiver operating characteristic (ROC).

Figs. 6 and 7 report the DOC in view of different value of the correlation coefficient ρ and the number of FTs M, respectively. In Fig. 6, one PT and two FTs are present, and we set SNR $=$ 0dB, $Q = 16$, $\rho = 0$, 0.2, 0.4, 0.6. In Fig. 7, one PT is considered, and SNR=0 dB, $Q = 16$, $\rho = 0.1$, $M = 2$, 4, 8.

From Figs. 6 and 7, some conclusions are briefly summarized as follows:

1. The larger P_l is set; the higher discrimination ratio is obtained. All curves in these figures pass through the origin,

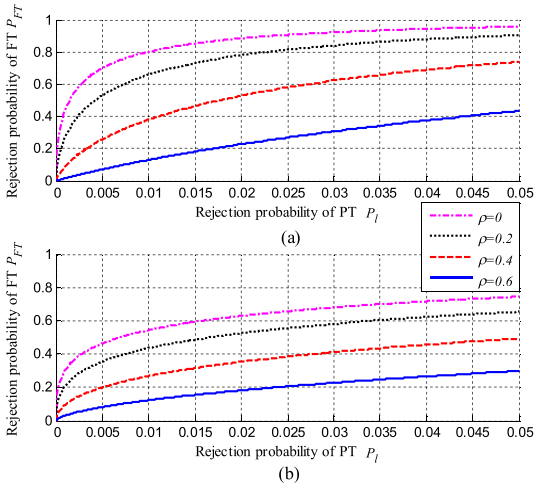

Fig. 6. Effect of varying ρ on DOC (SNR = 0dB, $Q = 16$, $M = 2$) in (a) case 1 and (b) case 2.

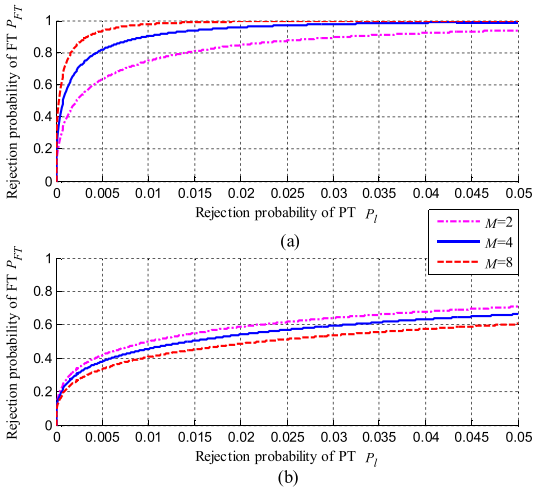

Fig. 7. Effect of varying M on DOC (SNR = 0dB, $Q = 16$, $\rho = 0.1$) in (a) case 1 and (b) case 2.

which represents that the threshold is set to be positive infinity in order to get $P_l = 0$.

2. Comparing both subfigures (a) with (b), the discrimination performance in case 1 is much better than that in case 2 with the same parameters, which shows that the random fluctuation of deception jamming can effectively improve the deception performance.

3. The discrimination performance for FTs becomes better with smaller correlation coefficient due to the increasing of the difference between PTs and FTs in spatial scattering properties.

4. In case 1, the more FTs are present; the higher discrimination ratio of FTs is obtained. On the contrary, the discrimination ability of FTs becomes even worse with the increasing number of FTs in case 2. This results from the conclusion that the identification ability of PTs exists under H_3 and H_4 in case 1, but exists under H_4 only in case 2.

C. Influence of Geometry Conditions

To analyze the influence of geometry conditions, we try to compare the discrimination performance of three different geometry conditions in a scenario with one PT and one deception FT. The positions of the transmitter X_T and receivers X_R^i are denoted on a common Cartesian coordinate system. The transmitter is always located at (0, 0). The locations of receivers are given below in meters.

Geometry 1: $X_R^1 = (300, 0)$, $X_R^2 = (-300, 0)$

Geometry 2: $X_R^1 = (100, 0)$, $X_R^2 = (-100, 0)$

Geometry 3: $X_R^1 = (300, 0)$, $X_R^2 = (-300, 0)$, $X_R^3 = (0, 300)$

The parameter of target size and carrier frequency are set to be the same with that of Fig. 2, i.e. D=15m, f_m=3GHz. The SNR of the target located at (0, 100)km is 0dB for every receivers. The SNR at other locations can be calculated by the bistatic radar equation. The beamwidth of every receiver is the same and set as $\theta_{3\text{dB}} = 0.5°$. Then the correlation coefficient of PT is determined by the relative location of receivers and targets and can be obtained by (7), and its estimation error depends on the angle accuracies of two receivers.

The expected rejection probability of PTs is set to be $P_l = 10^{-3}$ and 16 PRIs are used in our proposed method. For every point in the area $[-100, 100] \times [10, 100]$km, 5000 independent Monte Carlo runs are used to obtain the simulated rejection probability of FTs P_{FT} in the given three different geometries, which are reported in Fig. 8.

The location of targets affects the discrimination ability of the proposed method. When the target locates far away from the radar or out of the baseline of two receivers, the discrimination ability is reduced rapidly due to the increasing of correlation coefficient, which coincides with the previous analyzed results. Comparing Fig. 8(a) with Fig. 8(b), it can be seen that the discrimination performance becomes better with longer baseline of two receivers, which is caused by the effect of baseline on correlation coefficient. Compared with Fig. 8(a), the results in Fig. 8(c) is much better, since more receivers are used to discriminate deception jamming. Therefore, in order to obtain better discrimination performance, more receivers should be used and located dispersedly in the illuminated area of the jammer.

D. Comparison With Data Fusion-Based Method

In this section, a simulation is provided to verify the performance improvement of the proposed signal fusion-based method over the data fusion-based methods. The simulation scenario is the same with that of Fig. 8(a). Range deception is assumed and the deception range is set to 1000m. The bandwidth of transmitter signal is 5MHz. Fig. 9 shows the obtained rejection probability of FTs P_{FT} using the data fusion-based method.

Comparing Fig. 9 with Fig. 8(a), it is evident the proposed method outperforms the data fusion-based method, which demonstrates the performance improvement offered by signal fusion over data fusion. More remarkably, these two methods can be used in series. After implementing the signal fusion-based discrimination procedure, once a target has

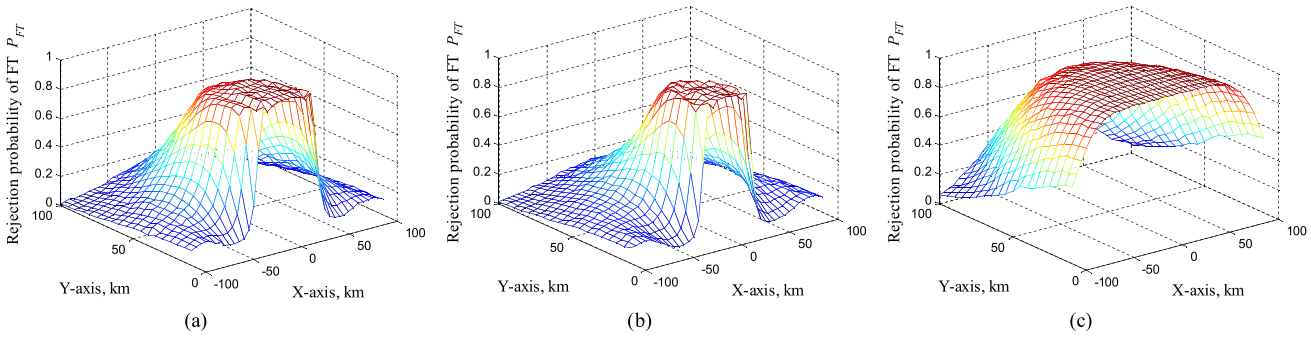

Fig. 8. Comparison of P_{FT} among three different geometries: (a) geometry 1, (b) geometry 2, and (c) geometry 3.

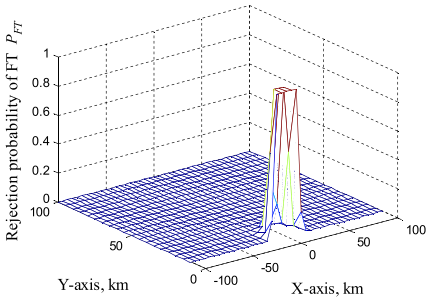

Fig. 9. Simulated P_{FT} using the data fusion-based method.

been discriminated as a FT, its measurement is ruled out immediately. On the contrary, if the target is judged as a PT, its measurement is preserved and be further discriminated using the data fusion-based method. In this way, better discrimination performance can be achieved.

VI. Conclusion

In this paper, a signal fusion-based algorithm is developed to discriminate deception jamming from radar targets in distributed multiple-radar architectures by making full use of their difference in spatial scattering properties. Invoking the Neyman-Pearson criterion, the proposed discrimination method is applied with a constant rejection probability of real targets. In addition, the theoretical expression for the rejection probability of false targets is derived. Both theoretical analysis and simulations verify the feasibility of the new algorithm, and its performance improvement over the data fusion-based methods is also demonstrated. Note that the new method works for the deception jamming with arbitrary modulation, and can be used in series with data fusion-based methods.

To limit the scope of the work, some simplified assumptions are made in this paper such as without considering the problem of synchronization among different receivers. Moreover, we consider mainly that all receivers are jammed and that the created false targets are fully correlated. When the correlation coefficient is less than one, further investigations should be performed in subsequent work. Another subsequent work is to develop a discrimination approach for the detection probability less than one.

References

[1] H. Godrich, A. P. Petropulu, and H. V. Poor, "Power allocation strategies for target localization in distributed multiple-radar architectures," *IEEE Trans. Signal Process.*, vol. 59, no. 7, pp. 3226–3240, Jul. 2011.

[2] E. Fishler, A. Haimovich, R. Blum, D. Chizhik, L. Cimini, and R. Valenzuela, "MIMO radar: An idea whose time has come," in *Proc. IEEE Radar Conf.*, Philadelphia, PA, USA, Apr. 2004, pp. 71–78.

[3] A. M. Haimovich, R. S. Blum, and L. J. Cimini, "MIMO radar with widely separated antennas," *IEEE Signal Process. Mag.*, vol. 25, no. 1, pp. 116–129, Jan. 2008.

[4] E. Fishler, A. Haimovich, R. S. Blum, L. J. Cimini, D. Chizhik, and R. A. Valenzuela, "Spatial diversity in radars-models and detection performance," *IEEE Trans. Signal Process.*, vol. 54, no. 3, pp. 823–838, Mar. 2006.

[5] V. S. Chernyak, *Fundamentals of Multisite Radar Systems: Multistatic Radars and Multistatic Radar Systems*. London, U.K.: CRC Press, 1998.

[6] P. Wang, H. Li, and B. Himed, "A parametric moving target detector for distributed MIMO radar in non-homogeneous environment," *IEEE Trans. Signal Process.*, vol. 61, no. 9, pp. 2282–2294, May 2013.

[7] I. Bekkerman and J. Tabrikian, "Target detection and localization using MIMO radars and sonars," *IEEE Trans. Signal Process.*, vol. 54, no. 10, pp. 3873–3883, Oct. 2006.

[8] H. Godrich, A. M. Haimovich, and R. S. Blum, "Target localization accuracy gain in MIMO radar-based systems," *IEEE Trans. Inf. Theory*, vol. 56, no. 6, pp. 2783–2803, Jun. 2010.

[9] D. C. Schleher, *Electronic Warfare in the Information Age*. Norwood, MA, USA: Artech House, 2000.

[10] A. Farina, "Electronic counter-countermeasures," in *Radar Handbook*, M. I. Skolnik, Ed., 3rd ed. New York, NY, USA: McGraw-Hill, 2008.

[11] S. D. Berger, "Digital radio frequency memory linear range gate stealer spectrum," *IEEE Trans. Aerosp. Electron. Syst.*, vol. 39, no. 2, pp. 725–735, Apr. 2003.

[12] N. Liu, S.-S. Zhao, and L.-R. Zhang, "A radar ECCM scheme based on full-rate orthogonal pulse block," *J. Comput. Inf. Syst.*, vol. 9, no. 24, pp. 9771–9779, 2013.

[13] J. Akhtar, "Orthogonal block coded ECCM schemes against repeat radar jammers," *IEEE Trans. Aerosp. Electron. Syst.*, vol. 45, no. 3, pp. 1218–1226, Jul. 2009.

[14] J. Zhang, D. Zhu, and G. Zhang, "New antivelocity deception jamming technique using pulses with adaptive initial phases," *IEEE Trans. Aerosp. Electron. Syst.*, vol. 49, no. 2, pp. 1290–1300, Apr. 2013.

[15] C. Huang, Z. Chen, and R. Duan, "Novel discrimination algorithm for deceptive jamming in polarimetric radar," in *Proc. ICITSE*, Berlin, Germany, 2013, pp. 359–365.

[16] B. Rao, Y.-L. Zhao, S.-P. Xiao, and X.-S. Wang, "Discrimination of exo-atmospheric active decoys using acceleration information," *IET Radar, Sonar Navigat.*, vol. 4, no. 4, pp. 626–638, Aug. 2010.

[17] B. Rao, S. Xiao, X. Wang, and T. Wang, "Maximum likelihood approach to the estimation and discrimination of exoatmospheric active phantom tracks using motion features," *IEEE Trans. Aerosp. Electron. Syst.*, vol. 48, no. 1, pp. 794–819, Jan. 2012.

[18] B. Rao, S. Xiao, and X. Wang, "Joint tracking and discrimination of exoatmospheric active decoys using nine-dimensional parameter-augmented EKF," *Signal Process.*, vol. 91, no. 10, pp. 2247–2258, Oct. 2011.

[19] M. Greco, F. Gini, and A. Farina, "Combined effect of phase and RGPO delay quantization on jamming signal spectrum," in *Proc. IEEE Int. Radar Conf.*, Arlington, VA, USA, May 2005, pp. 37–42.

[20] M. Greco, F. Gini, and A. Farina, "Radar detection and classification of jamming signals belonging to a cone class," *IEEE Trans. Signal Process.*, vol. 56, no. 5, pp. 1984–1993, May 2008.

[21] P. Stavroulakis, N. Farsaris, and T. D. Xenos, "Anti-jamming transmitter independent radar networks," in *Proc. ICSCN*, Chennai, India, Jan. 2008, pp. 269–273.
[22] L. Yang and Z.-K. Sun, "Identification of false targets in bistatic radar system," in *Proc. IEEE NAECON*, vol. 2. Dayton, OH, USA, Jul. 1997, pp. 878–883.
[23] Y.-L. Zhao, X.-S. Wang, G.-Y. Wang, Y.-H. Liu, and J. Luo, "Tracking technique for radar network in the presence of multi-range-false-target deception jamming," *Acta Electron. Sinica*, vol. 35, no. 3, pp. 454–458, 2007.
[24] B. Lv, Y. Song, and C.-Y. Zhou, "Study of multistatic radar against velocity-deception jamming," in *Proc. ICECC*, Ningbo, China, Sep. 2011, pp. 1044–1047.
[25] F. A. Butt, I. H. Naqvi, and A. I. Najam, "Radar ECCM against deception jamming: A novel approach using bi-static and mono-static radars," in *Proc. INMIC*, Islamabad, Pakistan, Dec. 2012, pp. 137–141.
[26] S. Zhou, H. Liu, Y. Zhao, and L. Hu, "Target spatial and frequency scattering diversity property for diversity MIMO radar," *Signal Process.*, vol. 91, no. 2, pp. 269–276, Feb. 2011.
[27] D. R. Brown and H. V. Poor, "Time-slotted round-trip carrier synchronization for distributed beamforming," *IEEE Trans. Signal Process.*, vol. 56, no. 11, pp. 5630–5643, Nov. 2008.
[28] W.-Q. Wang, "GPS-based time & phase synchronization processing for distributed SAR," *IEEE Trans. Aerosp. Electron. Syst.*, vol. 45, no. 3, pp. 1040–1051, Jul. 2009.
[29] Y. Yang and R. S. Blum, "Phase synchronization for coherent MIMO radar: Algorithms and their analysis," *IEEE Trans. Signal Process.*, vol. 59, no. 11, pp. 5538–5557, Nov. 2011.
[30] V. Y. Korolev and I. G. Shevtsova, "On the upper bound for the absolute constant in the Berry–Esseen inequality," *Theory Probab. Appl.*, vol. 54, no. 4, pp. 638–658, 2010.

Shanshan Zhao is currently pursuing the Ph.D. degree in signal processing at the National Laboratory of Radar Signal Processing, Xidian University, Xi'an, China.

Her research interests include statistical signal processing, information fusion in multisite radar system, and their application in radar electronic counter-countermeasure.

Linrang Zhang received the M.S. and Ph.D. degrees from Xidian University, Xi'an, China, in 1991 and 1999, respectively.

He is currently a Full Professor with the National Laboratory of Radar Signal Processing, Xidian University. His current research interests include radar signal processing, array signal processing, radar electronic counter-countermeasure, and radar imaging.

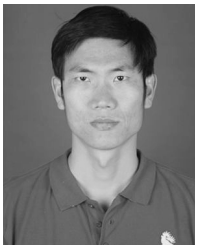

Yu Zhou received the M.S. and Ph.D. degrees from Xidian University, Xi'an, China, in 2004 and 2011, respectively.

He is currently an Associate Professor with the National Laboratory of Radar Signal Processing, Xidian University. His current research interests include statistical signal processing, cognitive radar signal processing, and multipleinput multipleoutput radar.

Nan Liu received the Ph.D. degree from Xidian University, Xi'an, China, in 2009. He is currently an Associate Professor with the National Laboratory of Radar Signal Processing, Xidian University. His current research interests include array signal processing, multipleinput multipleoutput radar, and radar electronic counter-countermeasure.